

# Correlations between second harmonic signal, microstructure, and mechanics of contracting collagen gels

Christopher B. Raub<sup>1</sup>, Peter D. Kim<sup>1</sup>, Andrew J. Putnam<sup>1,2</sup>, John S. Lowengrub<sup>3</sup>, Bruce J. Tromberg<sup>1,4,5</sup>, Steven C. George<sup>1,2</sup>

Department of Biomedical Engineering<sup>1</sup>, Department of Chemical Engineering and Materials Science<sup>2</sup>, Department of Mathematics<sup>3</sup>, The Beckman Laser Institute<sup>4</sup>, and Department of Surgery<sup>5</sup>, University of California, Irvine, Irvine, California

## ABSTRACT

Second harmonic generation (SHG) from collagen provides an optical signal that can yield detailed information about collagen microstructure when imaged with laser scanning microscopy, from both collagen-based engineered tissue and connective tissues from animals. Therefore SHG images may provide information that correlates with bulk tissue mechanical properties, or at least a component of those properties resulting from collagen. In order to probe these correlations, we used multiphoton microscopy to gather SHG signal intensity and depth decay information from fibroblast-seeded contracting collagen hydrogels. These gels were polymerized at pH 6 to engineer a tissue with large diameter collagen fibers and large pores between fibers, and pH 9 to produce smaller diameter collagen fibers with smaller pores. Both gels initially contained 4 mg/ml collagen; after 16 days of floating culture, the pH 6-polymerized gels had contracted to  $4.4 \pm 0.6\%$  of their original volume, and the pH 9-polymerized gels to  $10.7 \pm 2.7\%$ . During this time period, the bulk compressive moduli (CM) of the gels increased  $\sim 9.2$ -fold and  $\sim 1.4$ -fold for the pH 6 and pH 9 polymerization conditions, respectively. Correspondingly, the SHG signal at the tissue surface increased  $\sim 25$ -fold and  $\sim 19$ -fold for the pH 6 and pH 9 gels, respectively; whereas the effective SHG attenuation coefficient increased  $\sim 4.5$  and  $\sim 5.8$ -fold, respectively. Meaningful linear correlations only existed between the CM and surface SHG signal and the CM and SHG attenuation coefficient for pH 6-polymerized gels, indicating a possible influence of fibroblast activity on the CM of the pH-9 polymerized gels.

**KEYWORDS:** collagen, second harmonic, fibroblast, microstructure, tissue mechanics, compressive modulus

## 1. INTRODUCTION

Laser scanning multiphoton microscopy (MPM) provides a non-damaging, non-invasive means to image surface and shallow extracellular matrix microstructure in real and engineered tissues. The recent development of multiphoton and confocal endoscopes, which use fiber-optic based probes and miniaturized lens and scanning systems to enable two-photon imaging in a clinical setting, provide minimally invasive diagnostic opportunities in disease processes such as: diabetic crosslinking in skin, fibrosis and inflammation in airways, osteoarthritis in articular cartilage, and cancer metaplasia in colon, skin, and pancreas<sup>1, 2</sup>. Two signals often arise from multiphoton imaging of connective tissues: 1) second harmonic generation (SHG), a nonlinear process in which the noncentrosymmetric structure of collagen, myosin, tubulin, or SHG membrane dyes combines two incident photons into one scattered photon at half the incident frequency; and 2) two-photon autofluorescence (TPF) signal from elastin or intercellular fluorophores, excited with the same near infrared wavelength that produces SHG signal but emitted at longer Stokes-shifted wavelengths. Both SHG and TPF photons can be collected simultaneously providing endogenous contrast for imaging living connective tissue.

Multiphoton studies of collagen and elastin microstructure in visceral pericardium<sup>3</sup>, skin<sup>4-6</sup>, arteries and atherosclerotic plaques<sup>7-11</sup>, lung tissue,<sup>12</sup> and oral mucosa<sup>13</sup> have produced images of exquisite microstructural detail. However the pursuit of a quantitative relationship between the mechanical properties and the imaged microstructure remains largely unexplored. In diseases such as atherosclerosis, diabetes, asthma, chronic obstructive pulmonary disease, and emphysema, altered tissue mechanical properties contribute to disease symptoms and progression. Multiphoton imaging

of collagen and elastin structure in vivo holds promise as a minimally invasive way to predict absolute or relative values of tissue mechanical properties including tensile, compressive and shear moduli.

In order to better understand the relationship between MPM images, tissue microstructure, and mechanics our lab began with acellular collagen gels, manipulating the microstructure with gelation temperature<sup>14</sup> and pH<sup>15</sup>. We demonstrated that the bulk storage modulus is explained well using a microstructural mechanical model of the hydrogels as networks of entangled, semiflexible rods<sup>14, 16, 17</sup>. Although average fiber diameter and network mesh size were successfully extracted from SHG images of the collagen gels and used as input parameters for the microstructural model, these scaffolds differ considerably from most human tissues. For example, the collagen content in the gels was 0.4% by weight, whereas a typical pulmonary tissue is ~7% by weight collagen (ie, 70% of dry weight)<sup>18</sup>. Furthermore, the presence of cells would be expected to remodel the collagen network, changing the crosslinking, orientation and number density of fibers<sup>19</sup>; increasing local stress fields within the bulk tissue due to cell traction forces<sup>20, 21</sup>; contracting the entire matrix and increasing collagen concentration<sup>20</sup>; depositing collagen and other extracellular matrix components<sup>22</sup>; and also degrading collagen due to the secretion of matrix metalloproteases<sup>23</sup>.

In the current study we have added a stromal cell (normal human lung fibroblast, or NHLF) to the collagen gel which can directly manipulate the collagen architecture through new protein synthesis, and indirectly through gel contraction. We have tracked changes to the collagen microstructure using the SHG signal, and correlated changes in the microstructure and SHG signal with changes in bulk compressive moduli due to cell-induced remodeling and gel contraction. In addition, confocal fluorescence of immunostained NHLF-seeded collagen gels to reveals differences in fibroblast alpha-smooth muscle actin ( $\alpha$ -SMA) content, which may be explained as a response to the extracellular matrix stress environment created by cell traction forces.

## 2. METHODS

### 2.1 Collagen tissue construction

NHLFs (Lonza) were cultured in DMEM containing 10% fetal bovine serum, as well as basic fibroblast growth factor, insulin and gentamycin-A from a kit (Singlequot, Lonza) at concentrations determined by Lonza. 150 cm<sup>2</sup> polystyrene flasks housed the NHLFs, which were passaged upon reaching 70-80% confluence in monolayer culture. NHLFs in monolayer or in tissues were cultured under standard conditions in a humidified incubator kept at 37 °C and filled with air containing 5% CO<sub>2</sub>. Passage 6 NHLFs were trypsinized, counted with a hemacytometer, and seeded into collagen hydrogels of 0.5 ml volume at a concentration of 100,000 cells/ml. The collagen hydrogels were polymerized at 4 mg/ml and two different pH values, 6.0 and 9.0, by adding the following components to a sterile 50 ml tube (Corning) on ice: 1.2 ml of 10× concentrated PBS (Sigma) containing 0.19 mg/ml phenol red; 6.0 ml of sterile water with 0.005M or 0.03M sodium hydroxide for the pH 6 and pH 9-polymerized gels, respectively; 4.8 ml high concentration acid-soluble rat tail tendon collagen (BD Biosciences; concentration 10 mg/ml). After adding the latter three components on ice, sterile 50 ml tubes containing the gel components were mixed by gentle inversion and swirling by hand. Concentrated NHLFs, suspended after trypsinization in 0.2 ml of DMEM media, were added to each ice-cold collagen solution, and thoroughly mixed as before to achieve homogeneous cell density throughout the viscous solution. Finally, 0.5 ml of the collagen-NHLF solutions was pipetted into each well of two 24-well plates (Corning) and allowed to polymerize at room temperature (24 °C) for one hour, creating 24 tissues per polymerization condition. These tissues were then cultured in DMEM overnight. The tissues were then released from the wells by gently moving a sterile spatula between the gel and the plastic walls of the wells, and then allowing the gels to drop into DMEM in 13.5 cm-diameter Petri dishes. These floating gels were cultured in standard conditions for 16 days, during which time gels were periodically removed from the Petri dishes using a spoon-shaped sterile spatula for imaging, immunostaining, and mechanical testing. Three tissues each per polymerization condition were removed for multiphoton imaging immediately followed by mechanical testing on day 1, 2, 3, 6, 9, 12, and 16 of floating culture. These gels remained floating in DMEM before and after imaging, and were only resting on a coverslip during imaging ~10 minutes.

### 2.2 Multiphoton imaging

A Zeiss LSM 510 Meta multiphoton microscope was used for all imaging experiments. All SHG and two-photon fluorescence (TPF) signals were collected in the epi-configuration with an Achromplan 40×/0.8 NA water-immersion objective (Zeiss). Each 12-bit image contained 512×512 pixels, and each pixel was ~440 nm. Pixel sampling rate was

625 kHz; pixel dwell time was 1.6  $\mu$ s. NHLF-seeded collagen gels were placed on 22 $\times$ 50 mm No. 1 coverslips (170  $\mu$ m thickness) for imaging. SHG signal was produced by irradiating the sample with a focused circularly-polarized Chameleon laser tuned to 780 nm. Power before the objective was  $\sim$ 102 mW, and at the sample focus  $\sim$ 92 mW. SHG signal was collected using the instrument's meta detector, with wavelength cutoff points set at 383 nm and 394 nm. SHG images with signal averaged over 8 frames were collected 10  $\mu$ m deep into the tissue to provide the best assessment of collagen microstructure with the lowest signal-to-noise ratio. SHG images were also collected in serial depth sections ("z-stacks"), without frame-averaging and with 10  $\mu$ m between frames for a total of 11 frames, with the first frame 10  $\mu$ m above the bottom of the tissue. The lateral distance between fields of view was 1.1 mm, and three single image frames and three z-stacks were collected per tissue. Fibroblast two-photon autofluorescence was imaged by collecting the TPF signal with an infrared-blocking 535-590 nm bandpass filter.

### 2.3 Mechanical testing

After multiphoton imaging, NHLF-seeded collagen hydrogels were mechanically tested in unconfined compression using a Synergie 100 testing system (MTS Systems Corp.). The hydrogels were placed on a 50 mm diameter platen covered with 600-grade ultrafine waterproof sandpaper (3M), attached using double-sided scotch tape, to prevent slipping of the gel. Before testing, gel height and diameter were measured using a caliper and recorded. Each gel was compressed to 20% of the gel height with a 50 mm platen. Repeated compression cycles using the 50 mm platen tended to record lower compressive moduli due to syneresis, so only the first compression cycle was analyzed. For all platens, compression occurred at a rate of 0.05 mm/s and the resulting force was measured using a 10 N load cell. All compressive moduli were measured as the slope between 0 and 20% strain on the stress-strain curve, which was usually relatively linear between these points.

### 2.4 Immunofluorescence staining and imaging of $\alpha$ -SMA

Three tissues per polymerization condition were removed on day 3 of floating culture and fixed overnight at room temperature in PBS containing 4% formaldehyde. Following formaldehyde crosslinking of the NHLF-seeded collagen gels, the gels were rinsed 1 $\times$ 30 seconds + 3 $\times$ 10 minutes in PBS. The gels were then soaked overnight in PBS containing 2% (wt./vol.) glycine to react with any remaining unreacted formaldehyde, and further washed 3 $\times$ 10 minutes with PBS. The tissues were then permeabilized with 0.5% Triton-X in PBS for 10 minutes at room temperature. Following permeabilization, the gels were washed 3 $\times$ 10 minutes in TBS-T. Abdil was used as a blocking agent applied to the gels for 30 minutes at room temperature before incubation with the primary mouse anti- $\alpha$ -SMA monoclonal antibody (Sigma), for 70 minutes at room temperature at a concentration of X  $\mu$ g/ml. The gels were then washed 4 $\times$ 10 minutes in TBS-T. Incubation with the secondary goat anti-mouse Alexafluor 488-conjugated polyclonal antibody occurred for 70 minutes at room temperature in Abdil at an antibody concentration of Y  $\mu$ g/ml. Simultaneously, X mM DAPI was added to the secondary antibody solution in contact with the tissues. From this step onward, the tissues were protected from light. After washing away excess secondary antibody using 4 $\times$ 10 minute TBS-T washes, fluorescence was stabilized against photobleaching using 2 drops per tissue of antifade glycerol (Vectashield). The immunofluorescence signal was imaged with the Zeiss 510 Meta multiphoton microscope as mentioned above, except that lasers at both 488 nm and 800 nm were employed to create optical signals. The Alexafluor-488 labeled  $\alpha$ -SMA was excited at 488 nm and detected through a confocal pinhole and a 500-530 bandpass filter. Cell two-photon autofluorescence, collagen second harmonic, and DAPI TPF were generated using a laser at 800 nm wavelength and detected using a 535-590 nm bandpass filter, the meta filter set to collect between 393-404 nm, and a 395-465 nm bandpass filter, respectively.

### 2.5 Statistical analysis, image processing, and theoretical collagen concentration calculation

Correlations were assessed using the coefficient of determination ( $R^2$  value). All SHG signals were averages of single image frames, and were noise-subtracted. The average noise level was determined by averaging the intensities of sub-regions within single image frames which exclude collagen SHG signal. The theoretical collagen concentration was calculated from the gel height and diameter dimensions measured before mechanical testing, and by assuming that the gels were cylindrical and that the initial 2 mg mass of collagen per tissue was not significantly changed during floating culture. Some evidence supports both assumptions<sup>23</sup> (for example, see Figure 1; also unpublished data from acid-soluble collagen Sircol assays). All error bars represent standard deviation. Image processing including contrast and brightness enhancement for images within figures occurred similarly on all images presented.

### 3. RESULTS

#### 3.1 Collagen tissue contraction during floating culture

Once the NHLF-seeded collagen gels were established in floating culture, they quickly began contracting. The pH 6-polymerized gels rapidly contracted to less than 20% of their initial volume within 48 hours, whereas the pH 10-polymerized gels required more than 12 days to contract to less than 20% of the initial volume of 0.5 ml (Figure 1c). To the eye, the pH 6-polymerized gels were initially less transparent with higher albedo than the pH 9-polymerized gels (Figure 1a). The opacity of both sets of tissues increased as the gels contracted (Figure 1b). The microstructural reasons for these perceived differences are apparent in simultaneous SHG and TPF imaging of the tissues (Figure 1a,b): the increased fiber diameter of the pH 6-polymerized gels compared to the pH 9-polymerized gels as well as the increasing volume fraction of collagen fibers caused by fibroblast-mediated gel contraction both lead to increased tissue opacity, scattering and increased epi-detected SHG signal at the tissue surface. Unsurprisingly, the TPF signal (Figure 1a, b) reveals increased number density of fibroblasts as the gels contract, especially near the gel surface as has been previously observed<sup>20</sup>; and these cells may also contribute to the bulk tissue scattering properties<sup>24</sup>.

The rate of collagen gel contraction was rather constant for the pH 9-polymerized gels, whereas the pH 6-polymerized gels lost little additional volume after the first 48 hours (Figure 1c). By day 16 of floating culture, the pH 6-polymerized gels had contracted to  $4.4 \pm 0.6\%$  of their original volume, and the pH 9-polymerized gels to  $10.7 \pm 2.7\%$ .

Figure 1

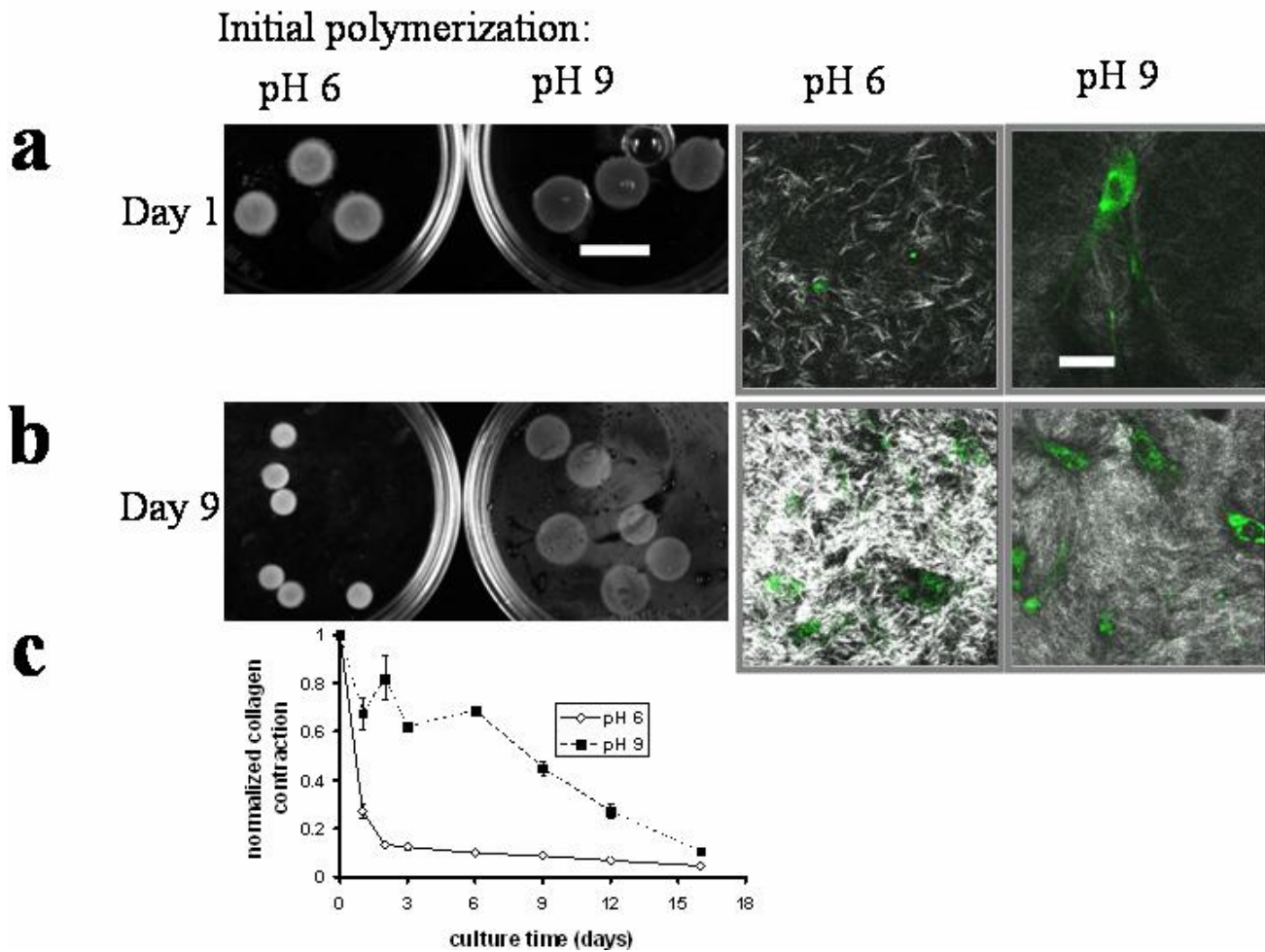


Figure 1. Digital photographs (on left) and representative MPM images (on right) of NHLF-seeded collagen gels after (a) 1 day and (b) 9 days floating culture. Bars represent 2 cm (on left) and 50  $\mu\text{m}$  (on right). NHLF autofluorescence signal is green and collagen SHG white in MPM images on right. (c) Collagen contraction during floating culture. Each data point is an average of three gels.

### 3.2 SHG intensity and decay increase during floating culture

Two commonly-measured image parameters include optical signal intensity near the surface of tissues and the signal depth decay. Both the SHG surface intensity (Figure 2a) and the SHG attenuation coefficient (Figure 2c) increase during floating culture. Expectedly, these parameters increase less quickly in the pH 9-polymerized gels, which contract to a lesser extent and at a slower rate than the pH 6-polymerized gels (for example SHG serial depth sections from day 1 for the pH 6 condition and day 12 for the pH 9 condition, see Figure 2b). At all time points during floating culture, a deeper imaging depth ( $>500 \mu\text{m}$  at day 1,  $>200 \mu\text{m}$  by day 16) was achieved into the pH 9-polymerized gels compared to the pH 6-polymerized gels ( $\sim 250 \mu\text{m}$  at day 1,  $\sim 100 \mu\text{m}$  by day 16). The slope of the best fit line of the surface SHG signal over culture time was  $\sim 2.6$ -fold larger for the pH 6 condition than the slope for the pH 9 condition. Similarly, the slope of the best fit line of the SHG attenuation coefficient over culture time was  $\sim 2.4$ -fold larger for the pH 6 condition than the slope for the pH 9 condition (slope and  $R^2$  values are found in the caption of Figure 2).

Figure 2

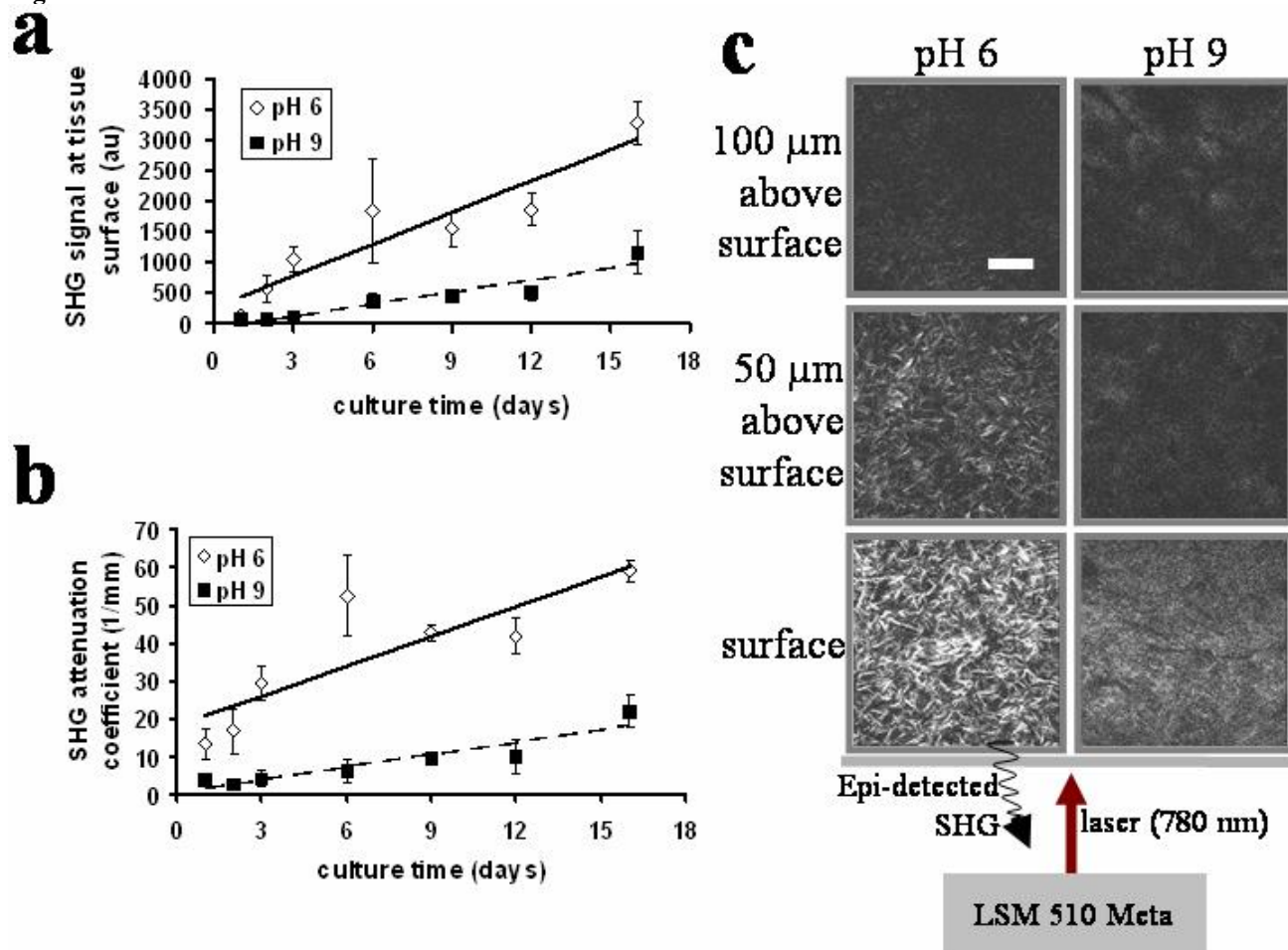


Figure 2. Epi-detected SHG (a) signal intensity at lower surface of NHLF-seeded collagen gels. The pH 6 best-fit line (solid) has slope  $m = 171$  arbitrary units (au)/day and  $R^2 = 0.87$ . The pH 9 best-fit line (dashed) has slope  $m = 66$  au/day and  $R^2 = 0.90$ . (b) Effective SHG attenuation coefficient of NHLF-seeded collagen gels during floating culture. The pH 6 best-fit line (solid) has slope  $m = 2.6 \text{ mm}^{-1}\cdot\text{day}^{-1}$  and  $R^2 = 0.72$ . The pH 9 best-fit line (dashed) has slope  $m = 1.1 \text{ mm}^{-1}\cdot\text{day}^{-1}$  and  $R^2 = 0.87$ . Each data point represents an

average of nine measurements from three gels. (c) Representative serial image planes from pH 6 and pH 9-polymerized gels after 1 and 11 days in culture, respectively (time points chosen to show similar signal decays).

### 3.3 Correlation between bulk compressive modulus (CM) and SHG signal

The bulk CM of NHLF-seeded collagen gels tended to increase throughout the 16 days of floating culture for the pH 6 condition, while in contrast the average CM of pH 9-polymerized gels peaked by day 3 of floating culture, and then decreased before exhibiting a recovery between day 12 and day 16 (Figure 3a). In pH 6-polymerized gels, variation in the average CM can be better explained by variation in average surface SHG signal (best-fit slope = 0.15 kPa/arbitrary unit (au),  $R^2 = 0.68$ ; Figure 3b) and average SHG attenuation coefficient (best-fit slope = 6.9 kPa·mm,  $R^2 = 0.40$ ; Figure 3c) than in the pH 9-polymerized gels. (best-fit slope = -0.01 kPa/au,  $R^2 = 0.15$ , Figure 3b; best-fit slope = -0.51 kPa·mm,  $R^2 = 0.011$ , Figure 3c).

Figure 3

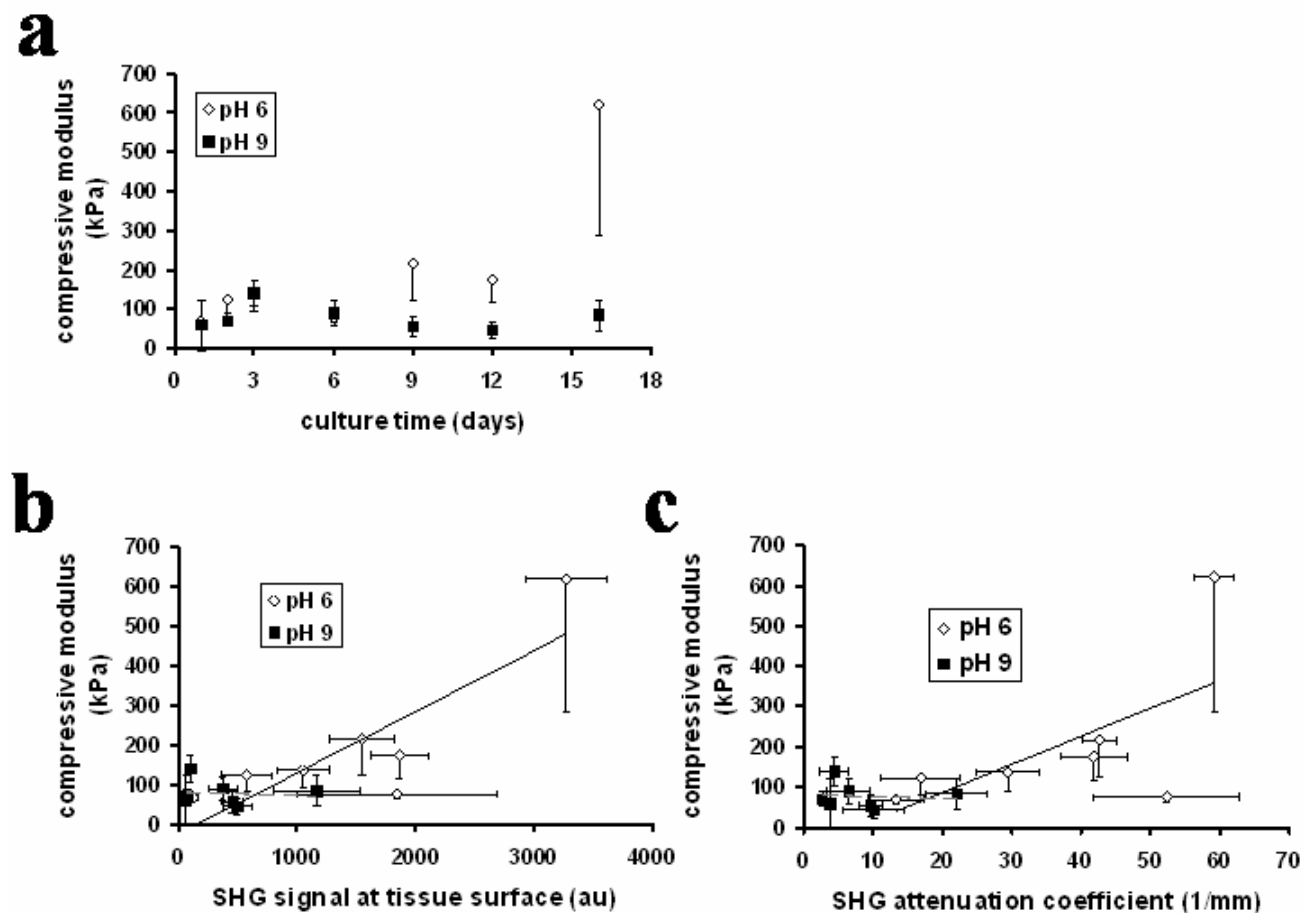


Figure 3. Bulk compressive moduli of NHLF seeded collagen gels (a) during floating culture, (b) correlating with mean surface SHG signal intensity, and (c) correlating with mean SHG signal attenuation coefficient from the tissues. Each data point represents 3-9 measurements from three gels. Solid lines represent the best-fit to the pH 6 condition; gray dashed lines represent the best-fit to the pH 9 condition.

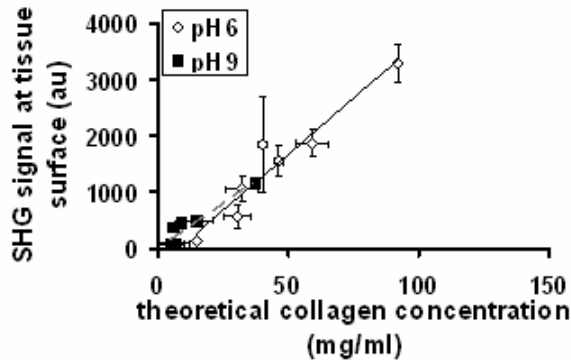
### 3.4 Collagen fiber size and fiber number density explain CM and SHG signal parameter trends

Although surface SHG signal and SHG depth decay do not correlate with the bulk CM of the slowly contracting pH 9-polymerized gels, variations in both of these image parameters are explained well by the variations in the theoretical collagen concentration of the tissues (Figure 4a, b). Interestingly, only after 16 days of culture do some of the fibroblast-seeded collagen gels begin to approach the concentrations of collagen found in animal lung tissue (~70 mg/ml). The

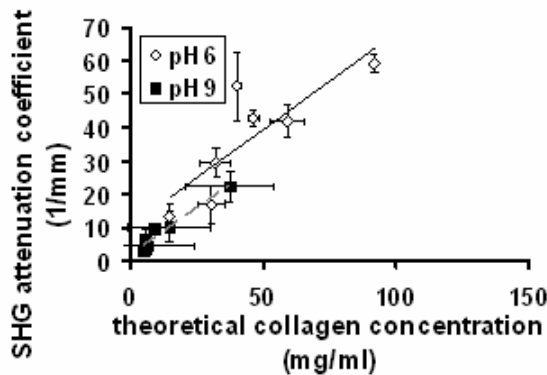
best-fit slope and  $R^2$  value of the correlation between surface SHG signal and collagen concentration are  $m = 39.7 \text{ au}\cdot\text{ml}\cdot\text{mg}^{-1}$  and  $R^2 = 0.92$  for the pH 6-polymerized gels and  $m = 31.3 \text{ au}\cdot\text{ml}\cdot\text{mg}^{-1}$  and  $R^2 = 0.89$  for the pH 9-polymerized gels (Figure 4a). The best-fit slope and  $R^2$  value of the correlation between SHG attenuation coefficient and collagen concentration are  $m = 0.58 \text{ ml}\cdot\text{mm}^{-1}\cdot\text{mg}^{-1}$  and  $R^2 = 0.55$  for the pH 6-polymerized gels and  $m = 0.69 \text{ ml}\cdot\text{mm}^{-1}\cdot\text{mg}^{-1}$  and  $R^2 = 0.94$  for the pH 9-polymerized gels (Figure 4b). The bulk CM of the pH 6-polymerized gels correlates with collagen concentration ( $m = 7.3 \text{ kPa}\cdot\text{ml}\cdot\text{mg}^{-1}$ ,  $R^2 = 0.68$ ), but the bulk CM of the pH 9-polymerized gels does not correlate ( $m = 0.09 \text{ kPa}\cdot\text{ml}\cdot\text{mg}^{-1}$ ,  $R^2 = 0.0006$ ).

Figure 4

**a**



**b**



**c**

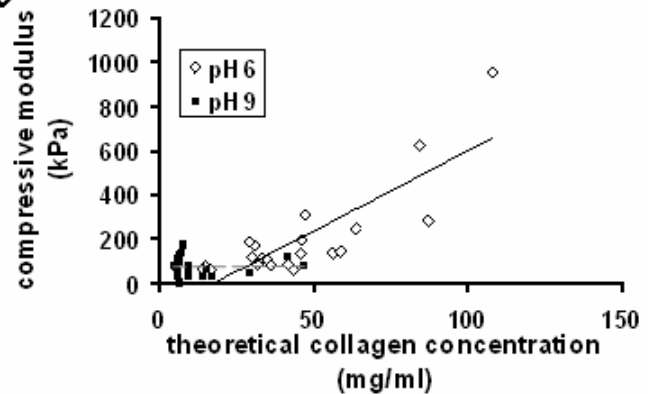


Figure 4. Correlation of (a) surface SHG signal intensity and (b) effective SHG attenuation coefficient with collagen concentration values determined from gel dimensions. Each data point represents 3-9 measurements from three gels. (c) Compressive modulus correlation with collagen concentration for pH 6 and pH 9-polymerized gels. Solid lines represent the best-fit to the pH 6 condition; gray dashed lines represent the best-fit to the pH 9 condition.

### 3.5 Collagen gel microstructure affects fibroblast $\alpha$ -SMA expression in floating culture

The polymerization pH-altered microstructure of collagen gels clearly affects the bulk mechanical properties (ie, CM) of the fibroblast-seeded gels (Figure 3a) as well as the rate at which the fibroblasts contract the gel (Figure 1c). Despite the bulk mechanical properties, which arise from the network of cells, collagen, and other matrix components as a whole, individual cells may interact with very localized mechanical properties of the surrounding matrix. To gain insight into the localized mechanical properties of the collagen gels experienced by the embedded fibroblasts, collagen tissues after 3 days in floating culture were fixed and stained for  $\alpha$ -SMA with indirect immunofluorescence. The bulk CM of these tissues were very similar (Figure 3a). Ten fibroblasts from two of the pH 6-polymerized gels were imaged; Figure 5a shows a representative fibroblast from this sample, with dim signal from the  $\alpha$ -SMA stain (Figure 5a, left-most column), a DAPI-stained nucleus (Figure 5a, central column), and a strong red-shifted two-photon autofluorescence signal (Figure 5a, right-most column, red signal) surrounded by large-diameter collagen fibers (Figure 5a, right-most column, white

SHG signal). In contrast, fibroblasts within a pH 9-polymerized gel had similarly uniformly bright autofluorescence and DAPI signals, although surrounded by dimmer, small-diameter collagen fibers (Figure 5b, central and right-most columns); but in contrast, the signal from the  $\alpha$ -SMA stain was quite bright though not observable as well-defined stress fibers. Figure 5c shows a control pH 9-polymerized tissue which was not incubated with primary antibody; subsequently, no image-forming signal was collected in the channel.

Figure 5

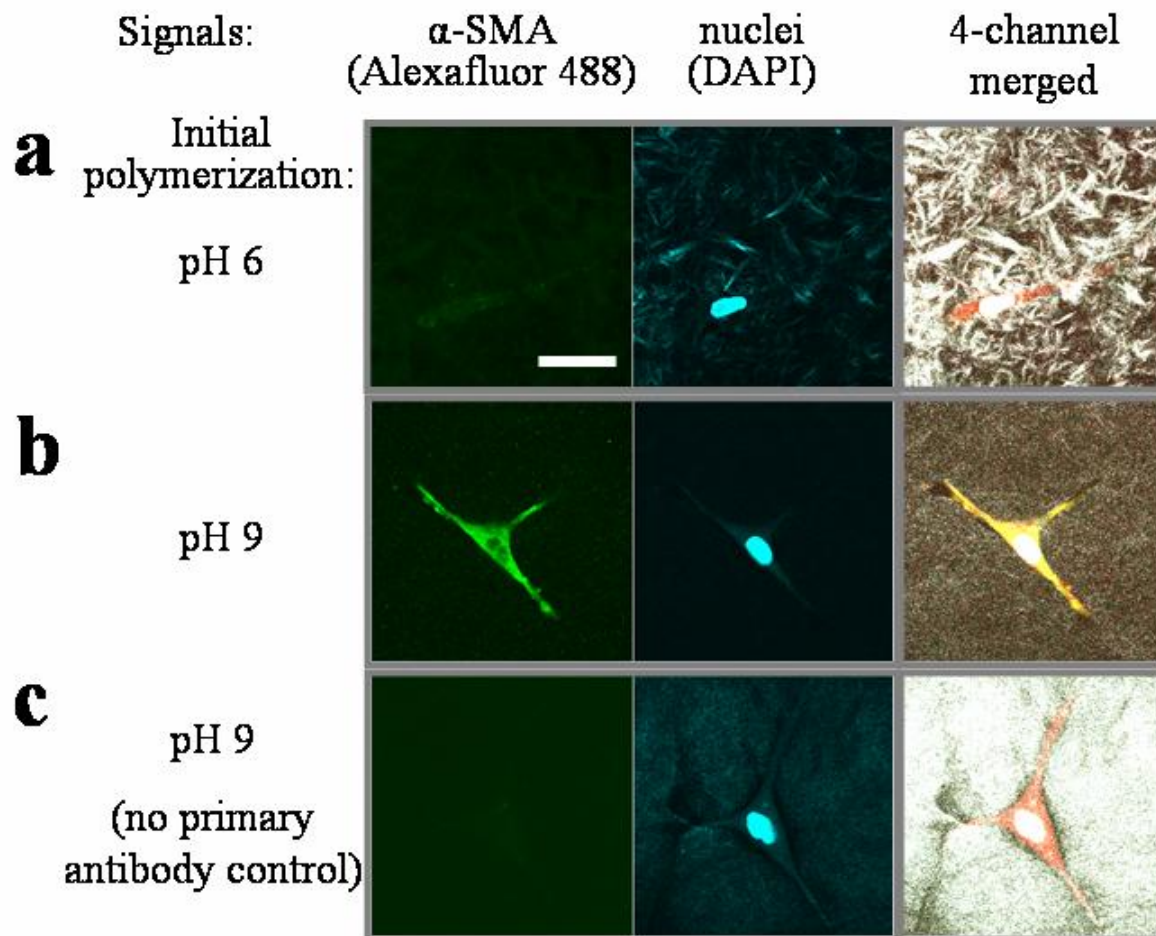


Figure 5. Indirect immunofluorescence staining of  $\alpha$ -SMA using mouse anti-SMA primary and Alexafluor 488-conjugated goat anti-mouse secondary antibody. The optical signals are Alexafluor-488 one-photon fluorescence (left-most column, green signal); DAPI TPF (central column, blue signal); fibroblast two-photon autofluorescence (right-most column, red signal); and collagen SHG (right-most column, white signal). (a) A representative image of a fibroblast from a pH 6-polymerized gel. (b) A representative image of a fibroblast from a pH 9-polymerized gel. (c) A representative image of a fibroblast from a pH 9-polymerized gel, incubated no primary antibody. Bar represents 50  $\mu$ m.

#### 4. DISCUSSION

We have previously published data describing correlations between two-photon signal (SHG and TPF) image parameters and bulk mechanical properties (storage and loss moduli) in acellular collagen hydrogels with polymerization pH and temperature-varied microstructures<sup>14, 15</sup>. These correlations showed that increasing collagen volume fraction and decreasing network mesh size tend to increase bulk stiffness of the gel and that these microstructural properties may be estimated from SHG images. We estimated the average network mesh size,  $L_M$  and mean fiber diameter,  $d$ , from SHG images. We then used a scaling relationship that predicts the bulk storage modulus ( $G'$ ) reasonably well, varying as:

$$G' \sim L_m^{-14/5} d^{-4/5} \quad (1).$$

This scaling relationship was derived from a model of an entangled network of semiflexible polymers<sup>16, 17</sup>. The present study attempts to extend the concept of relating bulk mechanical and optical properties from acellular collagen hydrogels to fibroblast-seeded dynamically contracting collagen gels, with collagen concentrations approaching those of *in vivo* tissues. The collagen gel contraction data are similar to other studies of human lung fibroblasts in collagen gels<sup>25-27</sup> but instead of changes in fibroblast cytoskeleton, in lysyl oxidase crosslinking, in cell density, or in collagen mass density altering gel contraction, these data suggest that stiffness arising from network entanglements inhibit collagen gel contraction (Figure 1). Presumably the larger collagen fibers polymerized at pH 6 are stiffer, but since the number density of fibers is less than at pH 9, the pH 6-polymerized gels are less entangled and more compliant to cell traction forces. While we cannot rule out increased apoptosis in the pH 9-polymerized gels leading to less collagen contraction, the cell population in those gels was easily visible under the light microscope and with MPM, and seemed numerous and devoid of large numbers of rounded apoptotic cells (Figure 1b). By day 16 the pH 6-polymerized gels were measured to have the largest bulk CM, and in fact the CM correlates well with SHG signal in these gels (Figure 3). Although the pH 9-polymerized gels displayed similar if less rapid increases in surface SHG intensity (Figure 2a) and SHG attenuation coefficient (Figure 2c), the correlations of these parameters with CM were poor. Certain blood-derived factors (ie, tumor necrosis factor, interleukin-6<sup>28</sup>, neutrophil elastase<sup>29</sup>, and interleukin-1 $\beta$  in tandem with thrombin<sup>23</sup>) can upregulate matrix metalloproteinase (MMP) activity in human lung fibroblasts, activity which could explain the decreased bulk CM of the pH 9-polymerized gels after three days floating culture. However, since no paracrine stimulation of MMP activity exists in these experiments, it is more likely that the mechanical environment in the pH 9-polymerized gels stimulates protease activity, concurrently with increased  $\alpha$ -SMA expression (Figure 5). The highly-entangled pH 9-polymerized gels resist deformation by cell traction forces, producing a mechanically loaded, stressed matrix, similar to collagen coated on polystyrene and anchored collagen gels, both of which have been shown to increase  $\alpha$ -SMA expression in fibroblasts relative to unanchored gels<sup>21</sup>. In contrast, the less entangled pH 6-polymerized gel is a more compliant tissue which tends to relax tension within the network, which correlates with decreased  $\alpha$ -SMA expression<sup>21</sup>. Similarly, anchored fibroblast-seeded collagen gels at least transiently (48 hours) express more MMP-3 and active MMP-9 than their floating counterparts<sup>30</sup>. This mechanism could explain the lowered CM of pH 9-polymerized gels after three days floating culture (Figure 3a).

The good correlations of surface SHG signal intensity (Figure 4a) and SHG attenuation coefficient (Figure 4b) with collagen concentration in both pH 6 and pH 9-polymerized gels suggests that these SHG signal parameters are sensitive to changes in collagen volume fraction within tissue, as well as to the scattering properties of single fibers.

In conclusion, the relationship between bulk mechanical properties and SHG signal may be somewhat confounded by variables related to cell-based remodeling of engineered tissue and animal connective tissue. TPF and confocal reflectance signals may yield additional information, especially about elastin and cellular organization in connective tissues. Additionally, a more complicated microstructural mechanical model than semiflexible network theory is needed to describe animal tissue with multiple extracellular matrix protein components, although semiflexible network theory may do well enough for some types of fibroblast-embedded contracting collagen gels. MPM imaging of collagen SHG signal should still provide accurate information concerning collagen concentration and microstructure, which are important determinants of the bulk mechanical properties of many connective tissues.

## 5. Acknowledgments

This work was supported, in part, by the National Institutes of Health (NIH # 442570-29181, SCG; F31 EB006677) This work was made possible, in part, through access to the Laser Microbeam and Medical Program (LAMMP) at the University of California, Irvine. The LAMMP facility is supported by the National Institutes of Health under a grant from the National Center for Research Resources (NIH # P41RR01192, BJT). In addition, we would like to thank the technical expertise and assistance of Dr. Tatiana Krasieva and Dr. Cyrus Ghajar for helpful scientific discussion and peer review.

## 6. References

1. Croix, C.S., W.R. Zipfel, and S.C. Watkins, "Potential solutions for confocal imaging of living animals". *Biotechniques*. **43**(1 Suppl): p. 14-9, 2007.

2. Konig, K., et al., "Clinical two-photon microendoscopy". *Microsc Res Tech.* **70**(5): p. 398-402, 2007.
3. Jobsis, P.D., et al., "Visceral Pericardium: Macromolecular structure and contribution to passive mechanical properties of the left ventricle". *Am J Physiol Heart Circ Physiol.* 2007.
4. Laiho, L.H., et al., "Two-photon 3-D mapping of ex vivo human skin endogenous fluorescence species based on fluorescence emission spectra". *J Biomed Opt.* **10**(2): p. 024016, 2005.
5. Koehler, M.J., et al., "In vivo assessment of human skin aging by multiphoton laser scanning tomography". *Opt Lett.* **31**(19): p. 2879-81, 2006.
6. Palero, J.A., et al., "Spectrally resolved multiphoton imaging of in vivo and excised mouse skin tissues". *Biophys J.* **93**(3): p. 992-1007, 2007.
7. Lilledahl, M.B., et al., "Characterization of vulnerable plaques by multiphoton microscopy". *J Biomed Opt.* **12**(4): p. 044005, 2007.
8. Le, T.T., et al., "Label-free molecular imaging of atherosclerotic lesions using multimodal nonlinear optical microscopy". *J Biomed Opt.* **12**(5): p. 054007, 2007.
9. Zoumi, A., et al., "Imaging coronary artery microstructure using second-harmonic and two-photon fluorescence microscopy". *Biophys J.* **87**(4): p. 2778-86, 2004.
10. Boulesteix, T., et al., "Micrometer scale ex vivo multiphoton imaging of unstained arterial wall structure". *Cytometry A.* **69**(1): p. 20-6, 2006.
11. Yu, W., et al., "In vivo imaging of atherosclerotic plaques in apolipoprotein E deficient mice using nonlinear microscopy". *J Biomed Opt.* **12**(5): p. 054008, 2007.
12. Pena, A.M., et al., "Three-dimensional investigation and scoring of extracellular matrix remodeling during lung fibrosis using multiphoton microscopy". *Microsc Res Tech.* **70**(2): p. 162-70, 2007.
13. Zhuo, S., et al., "The layered-resolved microstructure and spectroscopy of mouse oral mucosa using multiphoton microscopy". *Phys Med Biol.* **52**(16): p. 4967-80, 2007.
14. Raub, C.B., et al., "Noninvasive assessment of collagen gel microstructure and mechanics using multiphoton microscopy". *Biophys J.* **92**(6): p. 2212-22, 2007.
15. Raub, C.B., et al., "Image correlation spectroscopy of multiphoton images correlates with collagen mechanical properties". *Biophys J.* 2007.
16. Morse, D.C., "Viscoelasticity of Concentrated Isotropic Solutions of Semiflexible Polymers. 1. Model and Stress Tensor". *Macromolecules.* **31**: p. 7030-7043, 1998.
17. Morse, D.C., "Viscoelasticity of Concentrated Isotropic Solutions of Semiflexible Polymers. 2. Linear Response". *Macromolecules.* **31**: p. 7044-7067, 1998.
18. Francis, G. and J. Thomas, "Isolation and chemical characterization of collagen in bovine pulmonary tissues". *Biochem J.* **145**(2): p. 287-97, 1975.
19. Kostyuk, O. and R.A. Brown, "Novel spectroscopic technique for in situ monitoring of collagen fibril alignment in gels". *Biophys J.* **87**(1): p. 648-55, 2004.
20. Allen, T.D. and S.L. Schor, "The contraction of collagen matrices by dermal fibroblasts". *J Ultrastruct Res.* **83**(2): p. 205-19, 1983.
21. Arora, P.D., N. Narani, and C.A. McCulloch, "The compliance of collagen gels regulates transforming growth factor-beta induction of alpha-smooth muscle actin in fibroblasts". *Am J Pathol.* **154**(3): p. 871-82, 1999.

22. Gessin, J.C., et al., "Regulation of collagen synthesis in human dermal fibroblasts in contracted collagen gels by ascorbic acid, growth factors, and inhibitors of lipid peroxidation". *Exp Cell Res.* **206**(2): p. 283-90, 1993.
23. Fang, Q., et al., "Thrombin and TNF-alpha/IL-1beta synergistically induce fibroblast-mediated collagen gel degradation". *Am J Respir Cell Mol Biol.* **35**(6): p. 714-21, 2006.
24. Petroll, W.M., H.D. Cavanagh, and J.V. Jester, "Three-dimensional imaging of corneal cells using in vivo confocal microscopy". *J Microsc.* **170**(Pt 3): p. 213-9, 1993.
25. Redden, R.A. and E.J. Doolin, "Collagen crosslinking and cell density have distinct effects on fibroblast-mediated contraction of collagen gels". *Skin Res Technol.* **9**(3): p. 290-3, 2003.
26. Redden, R.A. and E.J. Doolin, "Complementary roles of microtubules and microfilaments in the lung fibroblast-mediated contraction of collagen gels: Dynamics and the influence of cell density". *In Vitro Cell Dev Biol Anim.* **42**(3-4): p. 70-4, 2006.
27. Zhu, Y.K., et al., "Contraction of fibroblast-containing collagen gels: initial collagen concentration regulates the degree of contraction and cell survival". *In Vitro Cell Dev Biol Anim.* **37**(1): p. 10-6, 2001.
28. Mikko, M., et al., "Human T cells stimulate fibroblast-mediated degradation of extracellular matrix in vitro". *Clin Exp Immunol.* 2007.
29. Fredriksson, K., et al., "Red blood cells increase secretion of matrix metalloproteinases from human lung fibroblasts in vitro". *Am J Physiol Lung Cell Mol Physiol.* **290**(2): p. L326-33, 2006.
30. Prajapati, R.T., et al., "Mechanical loading regulates protease production by fibroblasts in three-dimensional collagen substrates". *Wound Repair Regen.* **8**(3): p. 226-37, 2000.